ASME Journal of Applied Mechanics
Online journal at:
https://asmedigitalcollection.asme.org/appliedmechanics

Erteng Chen
Department of Mechanics and Engineering Science,
State Key Laboratory for Turbulence and Complex Systems,
College of Engineering,
Peking University,
Beijing 100871, China
e-mail: 309393@stu.xjtu.edu.cn

Zhaohe Dai[1]
Department of Mechanics and Engineering Science,
State Key Laboratory for Turbulence and Complex Systems,
College of Engineering,
Peking University,
Beijing 100871, China
e-mail: daizh@pku.edu.cn

Axisymmetric Peeling of Thin Elastic Films: A Perturbation Solution

We study the mechanical behavior of a thin elastic film that is affixed to a rigid substrate and subjected to a transverse force using a shaft with a finite radius. This scenario, also referred to as axisymmetric peeling, is encountered frequently in conventional blister tests as well as in our daily lives when removing an adhesive film from a substrate. Our primary objective is to gain a quantitative understanding of how the shaft's radius influences the relationships between force and displacement, as well as between force and delamination areas. These relationships can serve as a dependable method to determine both the film's elastic modulus and the adhesion strength between the film and its substrate. In this work, we provide a simple perturbation solution to this geometrically nonlinear problem while avoiding any use of ad hoc assumptions that were previously required. As a result, our results are in excellent agreement with numerical simulations and offer improved accuracy compared to analytical solutions available in the literature. [DOI: 10.1115/1.4062831]

Keywords: blister tests, adhesion, thin films, thin plates, 2D materials, elasticity, energy release rate, delamination, mechanical properties of materials

1 Introduction

Thin films with decreasing thickness have gained immense significance in a wide range of applications, from microelectromechanical systems to biomedical devices [1]. The mechanical and surface properties of thin films, such as Young's modulus and adhesion, play a crucial role in determining the reliability and functional performance of these thin films in various applications [2–4]. However, measuring these elastic and adhesive properties using conventional methods such as direct stretching and peeling is generally difficult, particularly for thin films with nanoscale thicknesses [1]. Instead, an alternative strategy is to exert a transverse force on the surface of a thin film to form a blister (also known as the blister test) [5–7]. In this test, the applied force causes the thin film to deflect out of the plane and peel axisymmetrically from the substrate [8]. Through experimental tools such as atomic force microscopy and scanning electron microscopy (SEM), the geometry of the blister, such as its height and lateral size, can be measured [9]. The interpretation of these measurements can provide quantitative insights into the elastic stiffness and adhesion strength of the tested film [10–14].

Accurately interpreting experimentally measured data on thin film blisters can be challenging due to the inherent nonlinearity in geometry [15,16]. To address this issue, extensive efforts have been dedicated to developing simple analytical solutions. For example, a Scherwrin-type solution that can satisfy the nonlinear governing equation of thin films has been derived. However, it is restricted to materials with a Poisson's ratio of 1/3 [12,17]. Williams analytically solved the nonlinear governing equations by assuming equal radial and hoop stresses throughout the span of the film [13]. Alternatively, Afferrante et al. made analytical progress by ignoring the in-plane displacement term [11]. Wan's solutions assumed a conical shape for the profile of the blister to remove the nonlinearity [10]. Similarly, the solution by Dai et al. took a power law for the shape of the blister [18]. Chandler and Vella solved a related indentation problem (peeling delamination is suppressed) and provided implicit solutions as well as their explicit forms for small indenter sizes [19]. More recently, Fang et al. discussed a model that combines the form of the Scherwrin-type solution and numerically examined prefactors [14]. However, obtaining these models has required various assumptions that in general constrain the accuracy of the resulting analytical solution.

In this work, our objective is to develop simple analytical solutions with improved accuracy for the axisymmetric peeling problem by avoiding the use of ad hoc assumptions. We begin in Sec. 2 by introducing the governing equations for the axisymmetric peeling (or blister test) problem. We also briefly discuss an exact solution (i.e., Scherwrin-type solution) that exists when the Poisson's ratio of the film is 1/3. In Sec. 3, we use a perturbation method to obtain the solution for the mechanical response of a thin film with pinned edges, with an arbitrary (yet allowable) Poisson's ratio. We then consider the effect of adhesion (unpinned edges) in Sec. 4 and compare our solutions to existing theories in Sec. 5.

2 Problem Description

In Fig. 1, we illustrate the axisymmetric peeling problem using a recent in situ experiment reported in Ref. [14] that measured the applied force to a thin film and the geometry of an axisymmetrically peeled blister. To describe this configuration, we consider an elastic film of thickness t, Young's modulus E, Poisson's ratio ν, and bending stiffness B adhered to a substrate with adhesion energy

[1]Corresponding author.

Manuscript received May 10, 2023; final manuscript received June 17, 2023; published online July 18, 2023. Assoc. Editor: Pradeep Sharma.

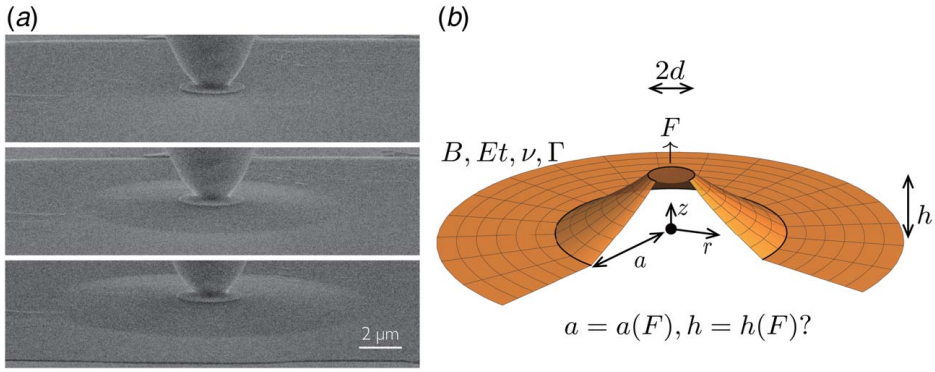

Fig. 1 Axisymmetric peeling of thin elastic films: (*a*) a series of in situ SEM images showing the peeling-off process of a ~100-nm-thick graphene from a gold substrate by a metal disk of radius *d* that is pulled away vertically by a micro-probe (courtesy of Fang et al. [14]) and (*b*) schematic illustration of the axisymmetric peeling problem and notions used in this work. The primary focus is on the relationship between the peeling force *F* and delamination radius *a* as well as between the peeling force and the peeling height *h*.

Γ. The film is pulled upwards by a flat-tip shaft in the region of $0 \leqslant r \leqslant d$ to produce an axisymmetric blister with delamination radius a and height h, as shown in Fig. 1(*b*). We assume that the physical size of the film is large enough so that its size will not influence the problem under study. It is important to note that force-displacement relationships have been well studied when a point load is applied ($d = 0$), for example in Refs. [7,17,19,20]. However, the point load is an oversimplified representation that does not fully reflect the loading conditions encountered in typical experiments such as that in Fig. 1(*a*). Particularly, in the early stage of peeling, the delamination radius is not large enough relative to the finite size of the loading zone. In addition, the use of the point load leads to stress singularity at the center (which is regularized by the finite loading size in practice) and results in non-trivial errors in the interpretation of experimental data including the force-displacement relationship (to be discussed later).

2.1 Theoretical Settings. We begin with a simple scenario in which the inner and outer edges of the blister at $r = d$ and $r = a$, respectively, are fixed. The objective is to examine the mechanical response of a film that is pulled up by a finite disc firmly bonded to the film, i.e., there is no slip in $0 \leqslant r \leqslant d$. We consider highly bendable or ultra-thin films such that the applied pulling force is balanced by the nonlinear tension of the film, following the membrane limit of the Föppl–von Kármán equations [4]. This only requires that the blister is sufficiently large ($h^2 \gg B/Et$). In this regard, the out-of-plane equilibrium equation is given by

$$-\frac{1}{r}\frac{\mathrm{d}}{\mathrm{d}r}\left(\frac{\mathrm{d}\varphi}{\mathrm{d}r}\frac{\mathrm{d}w}{\mathrm{d}r}\right) = \frac{F\delta(r-d)}{2\pi d} \tag{1}$$

where the Dirac function δ is used to represent the upward line force exerted on the circle at $r = d$ and φ is the Airy stress function. The in-plane equilibrium equation is automatically satisfied by linking in-plane stress resultants to the Airy stress function through

$$N_r = \frac{1}{r}\frac{\mathrm{d}\varphi}{\mathrm{d}r}, \quad N_\theta = \frac{\mathrm{d}^2\varphi}{\mathrm{d}r^2}$$

In addition, a compatibility equation is required to ensure a single-valued, continuous displacement field, i.e.,

$$\frac{1}{Et}\nabla_r^2\nabla_r^2\varphi = -\frac{1}{r}\frac{\mathrm{d}}{\mathrm{d}r}\left[\frac{1}{2}\left(\frac{\mathrm{d}w}{\mathrm{d}r}\right)^2\right] \tag{2}$$

where $\nabla_r^2 f = \frac{\mathrm{d}^2 f}{\mathrm{d}r^2} + \frac{1}{r}\frac{\mathrm{d}f}{\mathrm{d}r}$. This nonlinear problem is to be solved with no-slip boundary conditions at the inner and outer edges of the blister.

2.2 Nondimensionalization. Since the blister radius is fixed at this moment and the in-plane stiffness Et is invariant, it is natural to introduce the following nondimensionalization:

$$\rho = \frac{r}{a}, \quad W = \frac{w}{a}, \quad \Phi = \frac{\varphi}{Eta^2}, \quad \mathcal{F} = \frac{F}{Eta}, \quad H = \frac{h}{a}, \quad \eta = \frac{d}{a} \tag{3}$$

The dimensionless form of Eqs. (1) and (2) reads

$$-\Phi' W' = \frac{\mathcal{F}}{2\pi} \tag{4}$$

and

$$\rho\frac{\mathrm{d}}{\mathrm{d}\rho}\left[\rho\frac{\mathrm{d}}{\mathrm{d}\rho}(\rho\Phi')\right] = -\frac{1}{2}W'^2 \tag{5}$$

At the inner edge ($\rho = \eta$), we prescribe the blister height and have the no-slip condition

$$W(\eta) = H \quad \text{and} \quad \Phi''(\eta) - \frac{\nu}{\eta}\Phi'(\eta) = 0 \tag{6}$$

We also use $\Phi(\eta) = 0$ here since the specific value of the stress function is not important (only its derivative is of importance). At the outer edge ($\rho = 1$), we have zero deflection condition and again the no-slip condition

$$W(1) = 0 \quad \text{and} \quad \Phi''(1) - \nu\Phi'(1) = 0 \tag{7}$$

Equations (4) and (5) subject to boundary conditions (6) and (7) complete the problem discussed in this section.

2.3 Schwerin-Type Solution for $\nu = 1/3$. As discussed in Refs. [4,12], the classic Schwerin solution for a point load ($\eta = 0$) [21] can be obtained by searching a solution in the form $W = W(0)(1-\rho^o)$ and $\Phi = p\rho^q$. It was found that $o = 2/3$ and $q = 4/3$ can satisfy governing Eqs. (4) and (5) but the no-slip condition is satisfied only when $\nu = 1/3$ [4]. Along this line, a Schwerin-type solution for the case of finite η has also been obtained in Ref. [17]:

$$\overline{W} = W_0\left(1-\rho^{\frac{2}{3}}\right) \quad \text{and} \quad \overline{\Phi} = \frac{3}{16}W_0^2\rho^{\frac{4}{3}} \tag{8}$$

where

$$W_0 = H/\left(1-\eta^{2/3}\right)$$

according to the boundary condition (6). Plugging this solution into Eq. (4) immediately gives rise to a cubic force-displacement

relationship [17]

$$\alpha(\eta, \nu = 1/3) = \mathcal{F}/H^3 = \frac{\pi}{3}\left(1 - \eta^{2/3}\right)^{-3} \tag{9}$$

Note again that this relationship applies exclusively to thin films with $\nu = 1/3$ that happen to satisfy the no-slip boundary condition at both the inner and outer edges of the blister. We then move on to seek a solution that is valid for Poisson's ratios of any allowable value.

3 A Perturbation Solution

3.1 General Theory for $\nu \neq 1/3$ and $\eta \neq 0$. Moving on to arbitrary Poisson's ratio, it is natural to look for a small perturbation to the Schwerin-type solution (8) [12]. However, due to the finite inner radius of the suspended film studied here, directly obtaining the coefficients of the perturbation terms poses a challenge. Therefore, we opt for a variable substitution and then solve the perturbation terms, instead of relying on a complex matching process according to boundary conditions and power law relationships. Specifically, we utilize

$$\psi(\zeta) = \rho\Phi'(\rho), \quad \zeta = \rho^2 \tag{10}$$

to rewrite Eqs. (4) and (5) as

$$-\psi W_\zeta = \frac{\mathcal{F}}{4\pi} \tag{11}$$

and

$$\psi_{\zeta\zeta} = -\frac{1}{2} W_\zeta{}^2 \tag{12}$$

where the subscript ζ represents the derivative of the variable with respect to ζ. We then consider the perturbation term to the Schwerin-type solution (8)

$$W = \overline{W} + \widetilde{W} \quad \text{and} \quad \psi = \bar{\psi} + \widetilde{\psi} \tag{13}$$

with $|\widetilde{W}| \ll \overline{W}$ and $|\widetilde{\psi}| \ll \overline{\psi}$. Plugging Eq. (13) into Eqs. (11) and (12) and neglecting high-order terms we obtain a pair of simple perturbed governing equations

$$\widetilde{\psi}\overline{W}_\zeta + \widetilde{W}_\zeta\overline{\psi} = 0 \quad \text{and} \quad \widetilde{\psi}_{\zeta\zeta} + \overline{W}_\zeta\widetilde{W}_\zeta = 0 \tag{14}$$

Further combining Eqs. (8) and (14) yields an Euler equation for $\widetilde{\psi}$

$$\zeta^2\widetilde{\psi}_{\zeta\zeta} - \frac{4}{9}\widetilde{\psi} = 0 \tag{15}$$

Equation (15) can be directly solved with the no-slip boundary conditions at the inner and outer edges—which now become

$$\left[2\zeta\widetilde{\psi}_\zeta - (1+\nu)\widetilde{\psi} + \Delta\nu W_0{}^2\zeta^{2/3}\right]_{\zeta=\eta^2,1} = 0 \tag{16}$$

where

$$\Delta\nu = \frac{1-3\nu}{12} \tag{17}$$

is the small parameter associated with this perturbation method that ranges from -0.04 to 0.33 for $-1 \leqslant \nu \leqslant 0.5$. We will show shortly that the error of neglecting the high-order terms to obtain Eq. (14) is of the order of $\Delta\nu^2$.

Finally, we proceed to solve perturbation terms $\widetilde{\psi}$ and $\widetilde{W}$

$$\begin{aligned}\widetilde{\psi}(\rho) &= C_1\rho^{8/3} + C_2\rho^{-2/3} \quad \text{and} \\ \widetilde{W}(\rho) &= W_0\left[\frac{4}{3}C_1\left(\rho^2 - 1\right) - 2C_2\left(\rho^{-4/3} - 1\right)\right]\end{aligned} \tag{18}$$

and obtain the membrane deflection and complete stress function as

$$W(\rho) = W_0\left[1 - \rho^{2/3} + \frac{4}{3}C_1\left(\rho^2 - 1\right) - 2C_2\left(\rho^{-4/3} - 1\right)\right] \tag{19}$$

and

$$\Phi'(\rho) = \frac{1}{4}W_0{}^2\rho^{1/3} + C_1\rho^{5/3} + C_2\rho^{-5/3} \tag{20}$$

respectively, where C_1, C_2 are integration constants yet to be determined by specific boundary conditions. Though this perturbation method can be used for various cases including both no-slip and no-shear boundary conditions, at this moment we stick to the no-slip boundary condition (16) and find

$$C_1 = -\frac{D_2(\eta)}{(5/3-\nu)D_4(\eta)}\Delta\nu \quad \text{and} \quad C_2 = \frac{\eta^2 D_1(\eta)}{(5/3+\nu)D_4(\eta)}\Delta\nu \tag{21}$$

where $D_n(\eta) = 1 + \eta^{2/3} + \eta^{4/3} + \cdots + \eta^{2n/3}$. We also provide in Table 2 in Appendix B the asymptotic series of the constants C_1 and C_2 when the size of the loading zone η is small as well (in the late stage of the peeling).

It is clear from Eq. (21) that as ν approaches 1/3 and $\Delta\nu$ tends toward zero, Eqs. (19) and (20) return to the Schwerin-type solution (8) that is exact for $\nu = 1/3$. We note that Eq. (21) also indicates that our current solution is correct to the order of $\Delta\nu$ and the drop of quadratic terms in Eq. (14) corresponds to an error of $O(\Delta\nu^2)$ (which is within 1% for positive Poisson's ratio), justifying our assumption of a small perturbation. This level of error can also be shown by the comparison of our solution with numerical results in Table 1.

It is also worth noting that W_0 in these expressions is an intermediate parameter, rather than the height of the blister. The blister height can be evaluated by $H = W(\rho = \eta)$, leading to

$$H = A(\eta, \nu)W_0 \tag{22}$$

where

$$A(\eta, \nu) = \left(1 - \eta^{2/3}\right) + \left[\frac{4D_2(\eta)\left(1-\eta^2\right)}{(5-3\nu)D_4(\eta)} + \frac{6\eta^2 D_1(\eta)\left(1-\eta^{-4/3}\right)}{(5+3\nu)D_4(\eta)}\right]\Delta\nu \tag{23}$$

Therefore, for a given ν, η, and prescribed H, one can first solve for the parameter W_0 based on Eq. (22) and the constants C_1 and C_2 based on Eq. (21) and then obtain the shape and stress distribution in the film based on Eqs. (19) and (20) as well as the force required to make this blister based on Eq. (4).

3.2 Results and Discussion

3.2.1 Shape and Stress Distribution. We first examine this perturbation solution developed above by investigating the deflection of the thin film and the distribution of the Airy stress function in Fig. 2. These two quantities provide complete information about a blister. For verification purposes, we also numerically solve Eqs. (4) and (5) subject to (6) and (7) using regular boundary value problem solver such as `bvp4c` in MATLAB. We then compare numerical results (open markers in Fig. 2) with our analytical solution (dashed curves in Fig. 2).

Notably, for a given $\eta = d/a$, we can use the elementary geometry to approximate that the in-plane strain, ε, scales as h^2/a^2. Besides, given that the work done by the applied pulling force is converted into the strain energy stored in the film, we can readily have

$$\varepsilon \sim h^2/a^2, \quad Fh \sim Et\varepsilon^2 \times a^2 \quad \Rightarrow \quad \mathcal{F} \sim W^3 \sim \Phi'^{3/2} \tag{24}$$

Therefore, we present the plots of $W/\mathcal{F}^{1/3}$ and $\Phi'/\mathcal{F}^{2/3}$ as functions of ρ in Fig. 2 to eliminate the dependence of numerical results on the specific value of F used in the computation. Interestingly, after such rescaling, the Schwerin-type solution expressed in Eq. (8) exhibits a master curve with a shape that is independent of η for both deflection

Table 1 Comparison of the cubic force-displacement relationship (α) and linear blister height-radius relationship (φ) provided by different theories

		Force-displacement relationship		Adhesion effect		
		$\alpha = \mathcal{F}/H^3$		$h/a = \varphi(\Gamma/Et)^{1/4}$	$\Gamma a^2 = \beta Fh$	
References	Assumptions	$\alpha(\eta, \nu)$	Error	$\varphi(\eta, \nu)$	$\beta(\eta, \nu)$	Error
This work	–	Eq. (27) (Asymptotic, $\eta<0.2$)	0.22% (5.51%)	Eq. (33) (Asymptotic, $\eta<0.2$)	–	0.05% (0.05%)
Vella and Davidovitch [17]	$\nu = 1/3$	$\frac{\pi}{3}(1-\eta^{2/3})^{-3}$	21.08%	$\sqrt[4]{12}(1-\eta^{2/3})$	–	4.63%
Afferrante et al. [11]	No radial displacement	$\frac{8\pi}{27(1-\nu^2)}\left(\frac{1}{1-\eta^{2/3}}\right)^3$	7.63%	$\sqrt[4]{\frac{27(1-\nu^2)}{2}}(1-\eta^{2/3})$	–	1.78%
Wan [10]	Conical profile	$\frac{1-\eta^2-\eta\ln\eta^2}{4(1-\eta)^4/\pi}$	36.28%	$\left[\frac{8(1-\nu^2)(1-\eta)^5/\pi}{2(1-\eta^2)-\eta(\eta+3)\ln\eta^2}\right]^{1/4}$	–	46.89%
Williams [13]	Average stress	$\frac{\pi/(1-\nu)}{(1-\eta^2)\ln^2\eta}$	85.15%	–	$\frac{1}{4\pi}\left[\frac{1}{1-\eta^2}-\frac{2}{\ln\eta^2}\right]$	16.07%
Fang et al. [14]	Point indenter & Schwerin-type	$\varphi_0(\nu)(1-\eta^{2/3})^{-3}$	6.73%	–	$\frac{2\pi+(1-\nu^2)\alpha(\eta)(1-\eta)^3}{8\pi^2(1-\eta)}$	11.80%

Note: The maximum relative errors of all solutions are evaluated for $0\leqslant\nu\leqslant0.8$ and $0\leqslant\nu\leqslant0.5$, except for the asymptotic expansions of our perturbation solution, which are examined for small η, i.e., $0\leqslant\eta\leqslant0.2$.

and Airy stress function (see solid curves in Fig. 2). However, numerical results demonstrate a clear deviation from the Schwerin-type solution as well as a subtle dependence on η. Therefore, we rely on our perturbation solution given in Eqs. (19) and (20) which, despite their acceptable lengthiness, show excellent agreement with the numerical results (see dashed curves and markers in Fig. 2).

3.2.2 Relationship Between Force and Displacement. Focusing on the deflection and stress state of a thin film at each position is often unnecessary. Instead, the force-displacement curve provides a more direct measurement of the film's overall response. In this context, we demonstrate, using Eq. (24) and the perturbation solution, that the cubic force-displacement relationship can be expressed as

$$\mathcal{F} = \frac{\pi}{3}\left(\frac{H}{A}\right)^3 \tag{25}$$

and its dimensional form is

$$F = \alpha(\eta, \nu)Eth^3/a^2 \tag{26}$$

where $A = A(\eta, \nu)$ is defined in Eq. (23) and the coefficient α can be expressed as

$$\alpha = \frac{\pi}{3}\left\{\left(1-\eta^{2/3}\right) + \left[\frac{4D_2(\eta)\left(1-\eta^2\right)}{(5-3\nu)D_4(\eta)} + \frac{6\eta^2 D_1(\eta)\left(1-\eta^{-4/3}\right)}{(5+3\nu)D_4(\eta)}\right]\Delta\nu\right\}^{-3} \tag{27}$$

For experiments in which η is small, we provide an asymptotic expansion of the coefficient α in Eq. (A1) in Appendix A.

Figure 3 illustrates the relationship between the coefficient α and the ratio of the inner to the outer edge size, η. In Fig. 3(*a*), we observe that the numerical results match well with the solution obtained before and after perturbation when $\nu = 1/3$, as expected. Furthermore, Fig. 3(*b*) shows the coefficient for $\nu = 0$ and $\nu = 0.5$, which correspond to the two limiting cases of non-negative Poisson's ratios. Our perturbation solution given in Eq. (27) exhibits excellent agreement with numerical results over a wide range of η ($0\leqslant\eta\leqslant0.4$) shown in Fig. 3(*b*)) while the original Schwerin-type solution (red dashed curve) shows clear deviations.

4 Adhesion Effect

In the preceding section, we derived an analytical solution for the mechanical response of a thin film with fixed boundaries. However, in practical peeling experiments, the outer delamination radius is not predetermined or chosen arbitrarily. Instead, it is determined by the properties of interfacial adhesion and the applied peeling force. Hence, this section aims to investigate the criteria for interface delamination and the force-displacement response, taking into account adhesion, in greater detail.

4.1 A Delamination Condition. The variational principle provides a direct way to understand how the delamination radius is selected [22,23]. Consider the total energy of the system

$$\Pi = U_{elastic} + U_{external} + \pi\Gamma\left(a^2 - d^2\right) \tag{28}$$

where $U_{elastic}$ represents the strain energy stored in the suspended part of the film, $U_{external}$ represents the potential energy of external forces (which disappears during a displacement-control analysis), and $\pi\Gamma\left(a^2-d^2\right)$ represents surface energy term due to adhesion. A variational analysis $\delta\Pi = 0$ with $\delta d \neq 0$ can give the equilibrium Eqs. (1) and (2), together with a particular delamination boundary condition [22] similar to Kendall's 1D peeling angle [24]

$$N_r(1-\cos\theta_r) - \Gamma + \frac{1}{2}N_r\varepsilon_r = 0 \tag{29}$$

where N_r, θ_r, and ε_r are the radial stress, the acute angle between the film and the substrate, and the radial strain that are evaluated at the adhesion/delamination front ($r = a$), respectively.

Alternatively, delamination can be characterized as a process of separating the adhesion interfaces, enabling the application of the concept of Griffith's energy release rate [25–27]

$$\mathcal{G} = -\left.\frac{\mathrm{d}U_{elastic}}{\mathrm{d}A}\right|_h = -\left.\frac{\mathrm{d}}{\mathrm{d}A}\int_0^h F\,\mathrm{d}w\right|_h \tag{30}$$

where $\mathcal{G}$ denotes the amount of elastic energy released during the expansion of the delamination area to form new surfaces. Consequently, the delamination condition can be expressed as $\mathcal{G} = \Gamma$.

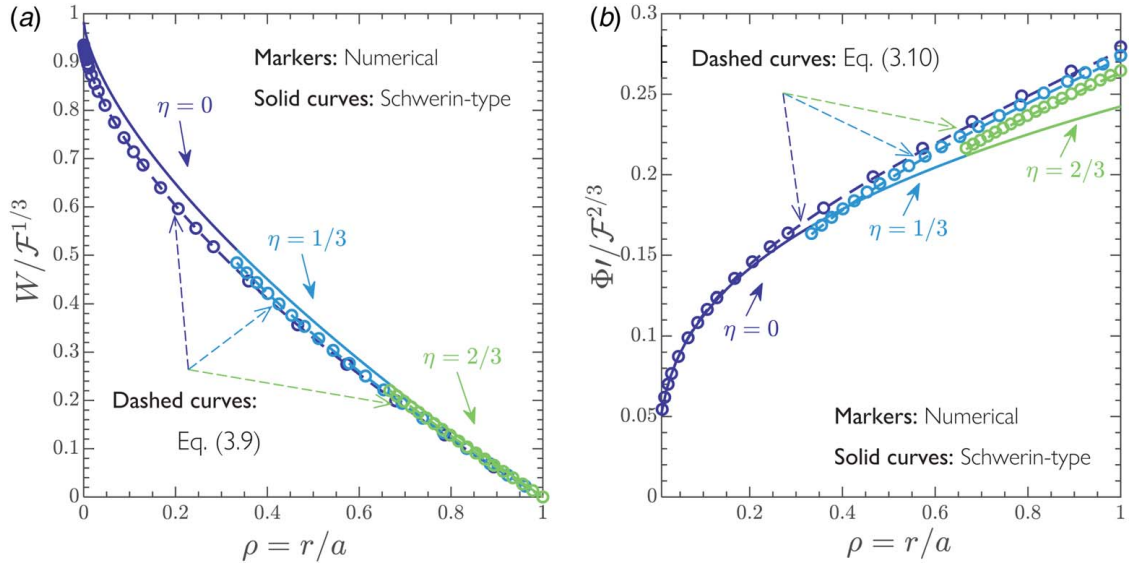

Fig. 2 (*a*) The deflection and (*b*) the derivative of the Airy stress function of an axisymmetrically peeled thin elastic film as functions of the rescaled radius position. The color denotes the ratio of the inner to the outer edge of the peeled blister: $\eta = 0$ (purple), $\eta = 1/3$ (blue), and $\eta = 2/3$ (green). Dashed curves denote our perturbation solution given in Eqs. (19) and (20), solid curves denote the Schwerin-type solution given in Eq. (8), and colored markers represent numerical results. The Poisson's ratio used here is 0.5.

We use both methods in subsequent calculations. Numerically, there is no discernible difference between the two, however, utilizing the boundary condition (29) enables easy computation of the critical adhesion energy under a prescribed H and η, which brings a great deal of convenience. On the other hand, the energy release rate method provides insight into the quality of an approximate solution throughout the entire domain, rather than solely at the outer boundary. Consequently, we use the first method to obtain numerical results and the second method to derive analytical results based on the perturbation solution we have discussed.

4.2 The Blister Height-Radius Relationship. We find that the balance between adhesive and elastic forces results in a characteristic blister height-to-radius ratio by combining Eqs. (24) and (30)

$$\Gamma \sim \frac{\mathrm{d}U_{elastic}}{\mathrm{d}A} \sim Et\left(\frac{h}{a}\right)^4 \tag{31}$$

We then use the perturbation solution presented in the previous section and the delamination condition (30) to derive the detailed prefactor for such scaling relation

$$\frac{h}{a} = \varphi(\eta, \nu)\left(\frac{\Gamma}{Et}\right)^{1/4} \tag{32}$$

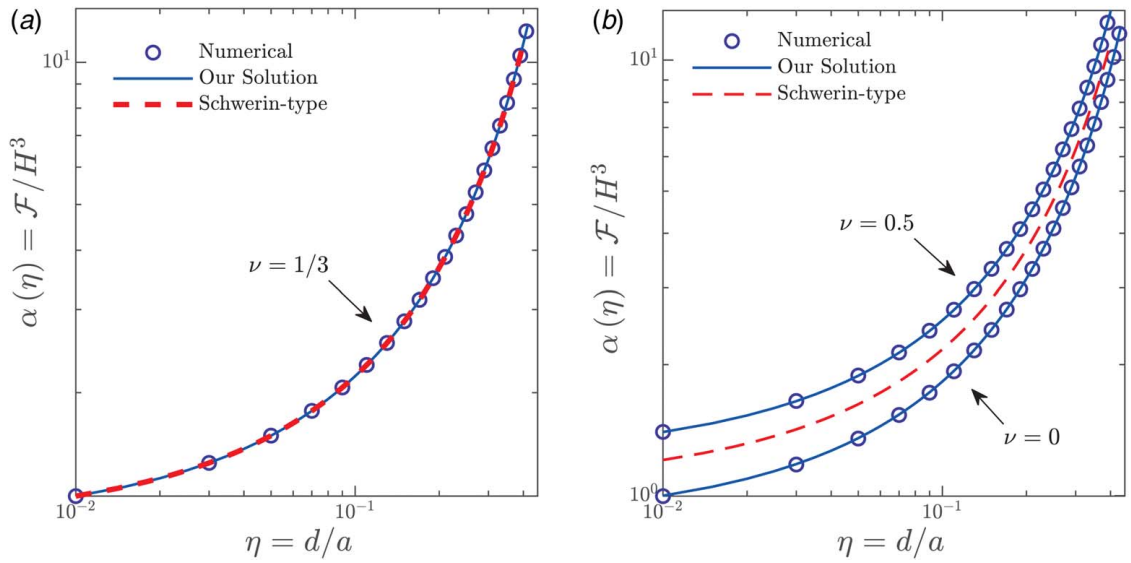

Fig. 3 Coefficient for the cubic force-displacement relationship as a function of $\eta = d/a$ for different Poisson's ratios: (*a*) $\nu = 1/3$ and (*b*) $\nu = 0.5$ and $\nu = 0$. The blue solid curves are given by Eq. (27) while red dashed curves are given by Eq. (9) that is exact only for $\nu = 1/3$. Note that the apparent stiffness of the thin film in all cases can be significantly increased by the size of the indenter or shafts.

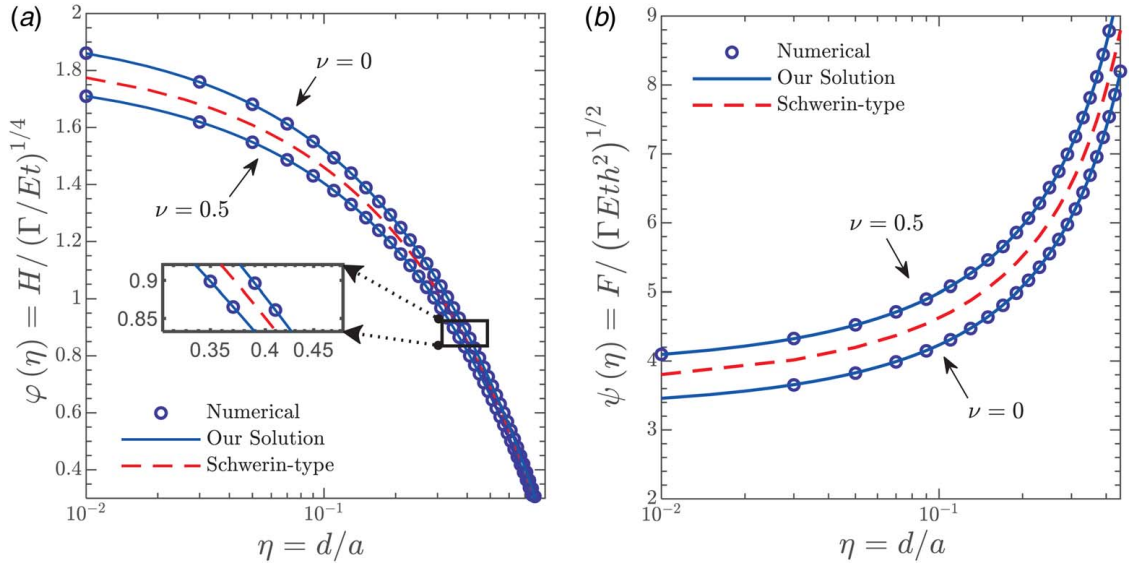

Fig. 4 The coefficient (*a*) φ for the blister height-radius relationship and (*b*) ψ for the linear force-height relationship as functions as η for two limiting Poisson's ratios. The solid curves in (*a*) and (*b*) are given by Eqs. (33) and (37), respectively while the dashed curves in (*a*) and (*b*) are from Schwerin-type solution given by Eqs. (34) and (38), respectively.

where

$$\varphi(\eta, \nu) = \left(\frac{24}{2A - 3\eta A_\eta}\right)^{1/4} A \tag{33}$$

the subscript η represents the derivative of the variable with respect to η, and the expression of A has been given in Eq. (23).

Equation (33) is not directly "user-friendly" due to the fractional expression involving η in A (we therefore provide the code for calculating it with given ν and η in GitHub). In addition, simplifications can be made when $\eta \ll 1$ using the asymptotic expansion of φ (see Eq. (A3) in Appendix A), which subjects to an error within 1% for $0 \leqslant \eta \leqslant 0.2$. In addition, the coefficient is found rather simple when $\nu = 1/3$

$$\varphi(\eta, \nu = 1/3) = 12^{1/4}\left(1 - \eta^{2/3}\right) \tag{34}$$

corresponding to the Schwerin-type solution (also see Table 1). In Fig. 4(*a*), we compare Eq. (33), the Schwerin-type solution for φ, and numerical results that are calculated using Eq. (29). Our perturbation solution agrees very well with numerical results for various Poisson's ratios over a large range of η (only two limits of non-negative Poisson ratios for $0 \leqslant \eta \leqslant 0.8$ are shown in Fig. 4(*a*)).

4.3 The Force-Height Relationship. We now revisit the force-displacement/height relationship by considering the delamination effect in the peeling process. Different from the pure indentation problem in which the boundary is fixed, the blister radius in the force-displacement relationship (27) varies with the applied force due to delamination. The work done by the indenter/shaft goes partly into the elastic energy stored in the film and partly into creating new surfaces. We then have

$$Fh \sim Et\varepsilon^2 \times a^2 \sim \Gamma \times a^2 \tag{35}$$

which can suggest a quasi-linear force-height relationship with the prefactor depending on the detailed ratio of the size of the inner to the outer edge, $\eta = d/a$, i.e.,

$$F = \psi(\eta, \nu)(Et\Gamma)^{1/2}h \tag{36}$$

Note that this quasi-linear behavior has been reported in the peeling experiments shown in Fig. 1(*a*) (see experimental data in Fig. 1(*e*) in Ref. [14]), which is distinct from the constant peeling force found by Gent and Kaang in the peeling of a 1D ribbon [28]. The coefficient can be directly calculated by combining Eqs. (26) and (32)

$$\psi(\eta, \nu) = \alpha\varphi^2 = \frac{\pi}{3A}\left(\frac{24}{2A - 3\eta A_\eta}\right)^{1/2} \tag{37}$$

where $A = A(\eta, \nu)$ has been given in Eq. (23). In Eq. (A4) in Appendix A, we also present the asymptotic expansion of Eq. (37) for small η. Moreover, ψ can be significantly simplified when $\nu = 1/3$, i.e.,

$$\psi(\eta, \nu = 1/3) = \frac{2\pi}{3^{1/2}}\left(1 - \eta^{2/3}\right)^{-1} \tag{38}$$

The comparison between Eqs. (37), (38), and numerics is shown in Fig. 4(*b*). Although this force-height relationship can be obtained straightforwardly from Eqs. (26) and (32), we have listed it separately here because of its significance in interpreting small-scale experiments where accessing the delamination area may not be feasible.

5 Summary of Different Theories and Conclusion

After discussing the perturbation solution for the axisymmetric peeling problem, we compare it with several references that have studied the peeling problem with finite loading radius considered [10,11,13,14,17]. Table 1 summarizes the explicit expressions for the key coefficients $\alpha(\eta, \nu)$ and $\varphi(\eta, \nu)$ provided in this work and the references, along with the assumptions used and the relative errors produced. We also include a parameter $\beta = \varphi^{-4}$ that characterizes the ratio of the adhesion energy to the work done by the applied force, since some references only reported β [13,14]. Additionally, we plot these α and φ as functions of η for a specific $\nu = 0.5$ in Fig. 5.

Table 1 and Fig. 5 clearly demonstrate the superior accuracy of our perturbation solution compared to others that often require certain assumptions. In addition, there are several insights that may not be immediately apparent, including:

- The conical profile assumption in Ref. [10] has a relatively small error when $\nu = 0$, when the coupling between the

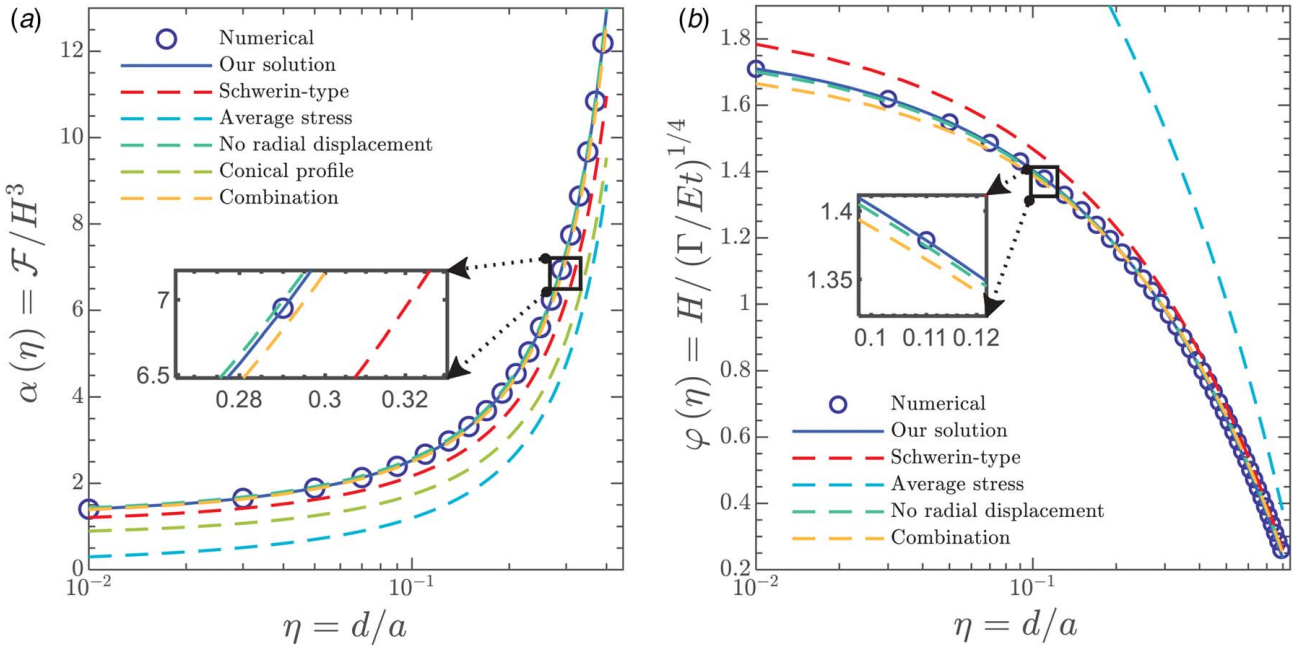

Fig. 5 The key coefficients α (*a*) and φ (*b*) obtained in this work and in the literature using various assumptions as functions of η. The detailed expressions of various solutions can be found in Table 1. $\nu = 0.5$ is used for demonstration purposes. Our solution is presented in Eqs. (27) and (33) for α and φ, respectively. Table 1 summarizes the expressions for other solutions, including "Schwerin-type" based on the solution by Vella and Davidovitch [17], "Average stress" given by Williams [13], "No radial displacement" given by Afferrante et al. [11], "conical profile" given by Wan [10], and "Combination" given by Fang et al. [14]

radial stress and hoop strain vanishes, and the blister shape approximates a straight line.

- The Schwerin-type solution is a special case of the solution given in Ref. [11] that assumes no radial displacement. Given its simplicity and relatively small error for $0 \leqslant \nu \leqslant 0.5$, we recommend the solution by Afferrante et al. [11] if the slip at the inner and outer edges of the blister is not too significant and the Poisson's ratio of the material is not too far from 1/3.
- When analyzing the shape or stress in the thin film or $\Delta\nu$ is not too small, we suggest using the perturbation solution presented here instead.
- In-plane displacement becomes important when slip occurs. In this case, both the Schwerin-type solution and the solution by Afferrante et al. can produce significant errors (see Fig. 6 in Appendix C). Instead, we recommend using the perturbation solution, which can adopt specific integration constants for various types of slip boundary conditions (see Table 2).

In conclusion, we have obtained an analytical solution for the axisymmetric peeling or blister problem by perturbing the Schwerin-type solution without making any assumptions about the physical background of the problem. Our solution provides a more accurate description of the film shape, stress distribution, and mechanical response of the thin film. The solution has a relatively concise form, and its coefficients can be flexibly adjusted based on different boundary conditions. Moreover, we anticipate that the method we used to obtain such a solution can be extended to consider other important factors, such as pre-tension, in future studies.

Acknowledgment

The authors are grateful for "The Fundamental Research Funds for the Central Universities (Peking University)" and the start-up funding from the College of Engineering (Peking University). The authors also gratefully acknowledge Zheng Fang and Xianlong Wei for providing raw SEM images.

Conflict of Interest

The authors declare that they have no known competing financial interests or personal relationships that could have appeared to influence the work reported in this paper.

Data Availability Statement

Mathematica code for calculating α and φ is available in GitHub.

Appendix A: Asymptotic Expansion of Several Coefficients

(1) *The coefficients of the asymptotic expansion of α.* For small $\eta \ll 1$, we can simplify the coefficient α in Eq. (27) by expanding it into

$$\alpha = g_\alpha(\nu)\left(\nu_0 + \nu_{2/3}\eta^{2/3} + \nu_2\eta^2 + \nu_{8/3}\eta^{8/3}\right) + \mathcal{O}\left(\eta^{10/3}\right) \tag{A1}$$

Here, the sake of notation convenience, we introduce

$$\Delta\nu_- = \frac{3}{5-3\nu}\Delta\nu \quad \text{and} \quad \Delta\nu_+ = \frac{3}{5+3\nu}\Delta\nu \tag{A2}$$

such that the prefactors in Eq. (A1) can be given as

$$g_\alpha(\nu)=\frac{1}{6}\pi,\quad \nu_0=\frac{54}{3+4\Delta\nu_-},\quad \nu_{2/3}=\frac{486(1+2\Delta\nu_+)}{(3+4\Delta\nu_-)^4},\quad \nu_{4/3}=\frac{2916(1+2\Delta\nu_+)^2}{(3+4\Delta\nu_-)^5}$$

$$\nu_2=\frac{45(1+2\Delta\nu_+)^3-2(3+4\Delta\nu_-)^2(3\Delta\nu_+-2\Delta\nu_-)}{(3+4\Delta\nu_-)^6/324}$$

$$\nu_{8/3}=\frac{486(1+2\Delta\nu_+)\left[135(1+2\Delta\nu_+)^3-16(3+4\Delta\nu_-)^2(3\Delta\nu_+-2\Delta\nu_-)\right]}{(3+4\Delta\nu_-)^7}$$

(2) *The coefficients of the asymptotic expansion of* . We expand the coefficient φ in Eq. (33) as

$$\varphi(\eta,\nu)=g_\varphi(\nu)\left(\nu_0+\nu_{2/3}\eta^{2/3}+\nu_2\eta^2+\nu_{8/3}\eta^{8/3}+\nu_{10/3}\eta^{10/3}\right)+\mathcal{O}\left(\eta^4\right) \tag{A3}$$

where the coefficients of each term are

$$g_\varphi(\nu)=\frac{1}{32\sqrt{3}(4-3\nu)^2(5+3\nu)^2}\left(\frac{4-3\nu}{5-3\nu}\right)^{3/4},$$

$$\nu_0=128\left(-20+3\nu+9\nu^2\right)^2$$

$$\nu_{2/3}=-48\left(1100-525\nu-621\nu^2+189\nu^3+81\nu^4\right),$$

$$\nu_2=-240(1-3\nu)^2\left(-20+3\nu+9\nu^2\right)$$

$$\nu_{8/3}=30(1-3\nu)^2\left(-55+18\nu+9\nu^2\right),$$

$$\nu_{10/3}=160(1-3\nu)^2\left(-20+3\nu+9\nu^2\right)$$

(3) *The coefficients of the asymptotic expansion of* ψ. We expand the coefficient ψ in Eq. (37) as

$$\psi(\eta,\nu)=g_\psi(\nu)\left(\nu_0+\nu_{2/3}\eta^{2/3}+\nu_2\eta^2+\nu_{8/3}\eta^{8/3}\right)+\mathcal{O}\left(\eta^{10/3}\right) \tag{A4}$$

where the coefficients of each term are

$$g_\psi(\nu)=\frac{6\pi}{(3+4\Delta\nu_-)^{11/2}},\ \nu_0=(3+4\Delta\nu_-)^4,$$

$$\nu_{2/3}=3(3+4\Delta\nu_-)^3(1+2\Delta\nu_+)$$

$$\nu_{4/3}=9(3+4\Delta\nu_-)^2(1+2\Delta\nu_+)^2,\ \nu_2=27(3+4\Delta\nu_-)(1+2\Delta\nu_+)^3$$

$$\nu_{8/3}=3(1+2\Delta\nu_+)\left[27+8\Delta\nu_-(3+4\Delta\nu_-)^2-54\Delta\nu_-\right.$$
$$\left.-96\Delta\nu_-\Delta\nu_+(3+2\Delta\nu_-)+324\Delta{\nu_+}^2+216\Delta{\nu_+}^3\right]$$

Appendix B: Coefficients Under Sliding Boundary Conditions

At the inner boundary, no-shear slippage can be characterized by that the region $0\leqslant\rho\leqslant\eta$ is in a uniform tension state. The corresponding boundary condition is

$$\eta\Phi''(\eta)-\Phi'(\eta)=0$$

This boundary condition may be applicable for material systems with slippery surfaces such as 2D materials [9,29,30] or lubricated surfaces [31]. At the outer boundary, we can obtain the corresponding no-shear boundary condition from the Lame solution assuming an infinite outer diameter

$$\Phi''(1)+\Phi'(1)=0$$

In Table 2, we show the key coefficients of the perturbation solution C_1 and C_2 as well as their asymptotic expansions using $\eta\ll1$ subject to various boundary conditions, including no-slip at both the inner and outer edge of the blister, slip only inside, slip only outside, and slip on both boundaries.

Appendix C: Mechanical Response Under Sliding Boundary Conditions

We examine a scenario where slip occurs at both the inner and outer boundaries, and compare the coefficients α and φ obtained through the perturbation method with those from the Schwerin-type solution and Afferrante et al.'s solution [11], alongside numerical results. To this end, we utilize C_1 and C_2 from Table 2 in this specific situation. For numerical results, we assume that the shear resistance between the film and substrate is zero (i.e., a frictionless interface). This allows the energy release rate method to be used for delamination conditions, while the critical boundary condition given by the variational method changes slightly [22,32]

$$N_r(1-\cos\theta_r)-\Gamma=0$$

Table 2 Summary of original expressions and asymptotic expansions of the integration constants in the perturbation solution under different boundary conditions

	C_1		C_2	
	Full expression	Asymptotic expansion	Full expression	Asymptotic expansion
No slip	Eq. (20)	$[1-\eta^2+\eta^{10/3}+\mathcal{O}(\eta^{16/3})]\Delta\nu_-$	Eq. (20)	$[\eta^2-\eta^{10/3}+\eta^{16/3}+\mathcal{O}(\eta^6)]\Delta\nu_+$
Slip inside	$\frac{4(1-3\nu)+\eta^2(5+3\nu)}{-16(5-3\nu)+4(5+3\nu)\eta^{10/3}}$	$-\frac{1-3\nu}{4(5-3\nu)}-\frac{5+3\nu}{16(5-3\nu)}\eta^2+\mathcal{O}(\eta^{10/3})$	$\frac{(5-3\nu)\eta^2+(1-3\nu)\eta^{10/3}}{-16(5-3\nu)+4(5+3\nu)\eta^{10/3}}$	$-\frac{1}{16}\eta^2-\frac{1-3\nu}{16(5-3\nu)}\eta^{10/3}+\mathcal{O}(\eta^{16/3})$
Slip outside	$\frac{-2(5+3\nu)+(1-3\nu)\eta^2}{80+48\nu-4(5-3\nu)\eta^{10/3}}$	$-\frac{1}{8}+\frac{1-3\nu}{16(5+3\nu)}\eta^2+\mathcal{O}(\eta^{10/3})$	$\frac{2(1-3\nu)\eta^2-(5-3\nu)\eta^{10/3}}{8(5+3\nu)-2(5-3\nu)\eta^{10/3}}$	$\frac{1-3\nu}{4(5+3\nu)}\eta^2-\frac{5-3\nu}{8(5+3\nu)}\eta^{10/3}+\mathcal{O}(\eta^{16/3})$
Slip on both boundaries	$-\frac{8+\eta^2}{4(16-\eta^{10/3})}$	$-\frac{1}{8}-\frac{1}{64}\eta^2-\frac{1}{128}\eta^{10/3}+\mathcal{O}(\eta^{16/3})$	$-\frac{2\eta^2+\eta^{10/3}}{2(16-\eta^{10/3})}$	$-\frac{1}{16}\eta^2-\frac{1}{32}\eta^{10/3}+\mathcal{O}(\eta^{16/3})$

Note: Note that the expressions of $\Delta\nu_-$ and $\Delta\nu_+$ have been given in Eq. (A2).

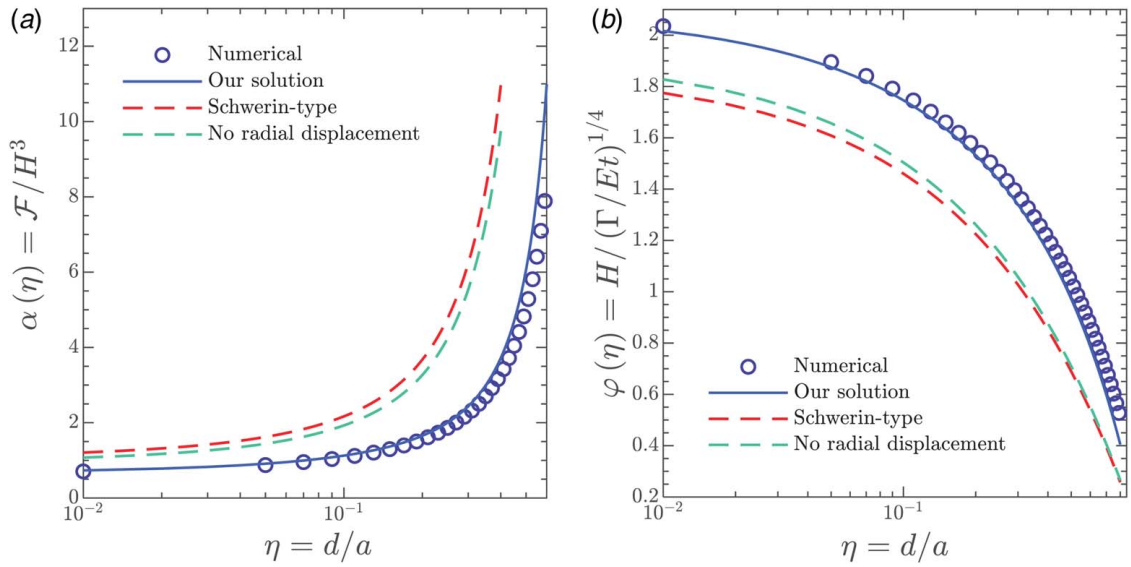

Fig. 6 Coefficients α (*a*) and φ (*b*) as functions of η under sliding boundary conditions at both the inner and outer edges of the blister. The Schwerin-type solution (which requires zero in-plane displacements at the boundary) and the solution by Afferrante et al. [11] (which essentially assumes no in-plane displacement) cannot be further refined. In contrast, the perturbation solution discussed in this work can utilize a pair of integration constants in Table 2 corresponding to the specific boundary conditions to achieve a much-improved agreement with numerical results.

As depicted in Fig. 6, both the Schwerin-type solution and Afferrante et al.'s solution have limited capability in interpreting the coefficients. On the other hand, our solution demonstrates good consistency with the numerical solution. However, since the error of the original solution is relatively large in this situation, our solution with leading-order correction exhibits an increased error compared to that in the situation of no slip.

References

[1] Freund, L. B., and Suresh, S., 2004, *Thin Film Materials: Stress, Defect Formation and Surface Evolution*, Cambridge University Press, Cambridge, UK.
[2] Dai, Z., Liu, L., and Zhang, Z., 2019, "Strain Engineering of 2D Materials: Issues and Opportunities at the Interface," Adv. Mater., **31**(45), p. 1805417.
[3] Akinwande, D., Brennan, C. J., Bunch, J. S., Egberts, P., Felts, J. R., Gao, H., Huang, R., et al., 2017, "A Review on Mechanics and Mechanical Properties of 2D Materials-Graphene and Beyond," Extreme Mech. Lett., **13**, pp. 42–77.
[4] Mansfield, E. H., 1989, *The Bending and Stretching of Plates*, Cambridge University Press, Cambridge, UK.
[5] Malyshev, B., and Salganik, R., 1965, "The Strength of Adhesive Joints Using the Theory of Cracks," Int. J. Fract. Mech., **1**, pp. 114–128.
[6] Dai, Z., Sanchez, D. A., Brennan, C. J., and Lu, N., 2020, "Radial Buckle Delamination Around 2D Material Tents," J. Mech. Phys. Solids, **137**, p. 103843.
[7] Dai, Z., and Lu, N., 2021, "Poking and Bulging of Suspended Thin Sheets: Slippage, Instabilities, and Metrology," J. Mech. Phys. Solids, **149**, p. 104320.
[8] Wan, K.-T., and Mai, Y.-W., 1996, "Fracture Mechanics of a Shaft-Loaded Blister of Thin Flexible Membrane on Rigid Substrate," Int. J. Fract., **74**(2), pp. 181–197.
[9] Dai, Z., Lu, N., Liechti, K. M., and Huang, R., 2020, "Mechanics at the Interfaces of 2D Materials: Challenges and Opportunities," Curr. Opin. Solid State Mater. Sci., **24**(4), p. 100837.
[10] Wan, K.-T., 2001, "Adherence of an Axisymmetric Flat Punch on a Thin Flexible Membrane," J. Adhes., **75**(4), pp. 369–380.
[11] Afferrante, L., Carbone, G., Demelio, G., and Pugno, N., 2013, "Adhesion of Elastic Thin Films: Double Peeling of Tapes Versus Axisymmetric Peeling of Membranes," Tribol. Lett., **52**(3), pp. 439–447.
[12] Chopin, J., Vella, D., and Boudaoud, A., 2008, "The Liquid Blister Test," Proc. R. Soc. A, **464**(2099), pp. 2887–2906.
[13] Williams, J., 1997, "Energy Release Rates for the Peeling of Flexible Membranes and the Analysis of Blister Tests," Int. J. Fract., **87**(3), pp. 265–288.
[14] Fang, Z., Dai, Z., Wang, B., Tian, Z., Yu, C., Chen, Q., and Wei, X., 2023, "Pull-to-Peel of Two-Dimensional Materials for the Simultaneous Determination of Elasticity and Adhesion," Nano Lett., **23**(2), pp. 742–749.
[15] Gent, A., and Lewandowski, L., 1987, "Blow-Off Pressures for Adhering Layers," J. Appl. Polym. Sci., **33**(5), pp. 1567–1577.
[16] Audoly, B., and Pomeau, Y., 2010, *Elasticity and Geometry: From Hair Curls to the Nonlinear Response of Shells*, Oxford University Press, Oxford, UK.
[17] Vella, D., and Davidovitch, B., 2017, "Indentation Metrology of Clamped, Ultra-Thin Elastic Sheets," Soft. Matter., **13**(11), pp. 2264–2278.
[18] Dai, Z., Hou, Y., Sanchez, D. A., Wang, G., Brennan, C. J., Zhang, Z., Liu, L., and Lu, N., 2018, "Interface-Governed Deformation of Nanobubbles and Nanotents Formed by Two-Dimensional Materials," Phys. Rev. Lett., **121**(26), p. 266101.
[19] Chandler, T. G., and Vella, D., 2020, "Indentation of Suspended Two-Dimensional Solids: The Signatures of Geometrical and Material Nonlinearity," J. Mech. Phys. Solids, **144**, p. 104109.
[20] Komaragiri, U., Begley, M., and Simmonds, J., 2005, "The Mechanical Response of Freestanding Circular Elastic Films Under Point and Pressure Loads," J. Appl. Mech., **72**(2), pp. 203–212.
[21] Schwerin, E., 1929, "Über Spannungen und Formänderungen Kreisringförmiger Membranen," Zeitschrift angewandte Mathematik und Mechanik, **9**(6), pp. 482–483.
[22] Dai, Z., Rao, Y., and Lu, N., 2022, "Two-Dimensional Crystals on Adhesive Substrates Subjected to Uniform Transverse Pressure," Int. J. Solids Struct., **257**, p. 111829.
[23] Rao, Y., Kim, E., Dai, Z., He, J., Li, Y., and Lu, N., 2023, "Size-Dependent Shape Characteristics of 2D Crystal Blisters," J. Mech. Phys. Solids, **175**, p. 105286.
[24] Kendall, K., 1975, "Thin-Film Peeling—The Elastic Term," J. Phys. D: Appl. Phys., **8**, p. 1449.
[25] Long, R., and Hui, C.-Y., 2012, "Axisymmetric Membrane in Adhesive Contact With Rigid Substrates: Analytical Solutions Under Large Deformation," Int. J. Solids Struct., **49**, pp. 672–683.
[26] Johnson, K. L., Kendall, K., and Roberts, A. D., 1971, "Surface Energy and the Contact of Elastic Solids," Proc. R. Soc. Lond. A, **324**(1558), pp. 301–313.
[27] Griffith, A. A., 1921, "VI. The Phenomena of Rupture and Flow in Solids," Philos. Trans. Royal Soc. A, **221**(582–593), pp. 163–198.
[28] Gent, A., and Kaang, S., 1986, "Pull-Off Forces for Adhesive Tapes," J. Appl. Polym. Sci., **32**(4), pp. 4689–4700.
[29] Lou, L., Chen, P., Wang, Z., Zhang, S., and Gao, F., 2020, "Cohesive Energy Measurement of Van Der Waals Heterostructures by the Shaft Loaded Blister Test," Extreme Mech. Lett., **41**, p. 100987.
[30] Zhang, K., and Arroyo, M., 2017, "Coexistence of Wrinkles and Blisters in Supported Graphene," Extreme Mech. Lett., **14**, pp. 23–30.
[31] Dai, Z., and Vella, D., 2022, "Droplets on Lubricated Surfaces: The Slow Dynamics of Skirt Formation," Phys. Rev. Fluids, **7**(5), p. 054003.
[32] Yang, X., Srivastava, A., and Long, R., 2023, "Adhesive Contact of an Inflated Circular Membrane With Curved Surfaces," Int. J. Solids Struct., **279**, p. 112371.